GBSS mutations in an *SBE* mutated background restore the potato starch granule morphology and produce ordered granules despite differences to native molecular structure

Shishanthi Jayarathna [a,*], Per Hofvander [b], Zsuzsanna Péter-Szabó [c], Mariette Andersson [b], Roger Andersson [a]

[a] Department of Molecular Sciences, BioCenter, Swedish University of Agricultural Sciences, P.O. Box 7015, SE-750 07 Uppsala, Sweden
[b] Department of Plant Breeding, Swedish University of Agricultural Sciences, P.O. Box 190, SE-23422 Lomma, Sweden
[c] Division of Glycoscience, Department of Chemistry, KTH-Royal Institute of Technology, SE-10621 Stockholm, Sweden

ARTICLE INFO

ABSTRACT

Potato starch with mutations in starch branching enzyme genes (*SBEI, SBEII*) and granule-bound starch synthase gene (*GBSS*) was characterized for molecular and thermal properties. Mutations in *GBSS* were here stacked to a previously developed *SBEI* and *SBEII* mutation line. Additionally, mutations in the *GBSS* gene alone were induced in the wild-type variety for comparison. The parental line with mutations in the *SBE* genes showed a ~ 40 % increase in amylose content compared with the wild-type. Mutations in *GBSS-SBEI-SBEII* produced non-waxy, low-amylose lines compared with the wild-type. An exception was a line with one remaining *GBSS* wild-type allele, which displayed ~80 % higher amylose content than wild-type. Stacked mutations in *GBSS* in the *SBEI-SBEII* parental line caused alterations in amylopectin chain length distribution and building block size categories of whole starch. Correlations between size categories of building blocks and unit chains of amylopectin were observed. Starch in *GBSS-SBEI-SBEII* mutational lines had elevated peak temperature of gelatinization, which was positively correlated with large building blocks.

1. Introduction

The main component of potato tubers besides water is starch, which accounts for 15–20 % of the weight. Potato starch is composed of two macromolecules, amylose and amylopectin. Amylose is principally a linear chain molecule with a degree of polymerization (DP) in the order of 2000–5000 residues (Hoover, 2001) and accounts for 20–30 % of potato starch (Bertoft & Blennow, 2016). The highly branched amylopectin molecules are composed of two types of chains, defined as long (L) and short (S), which differentiate at DP 36 (Bertoft, 2017). Other than L and S chains, some starch types were reported to contain extralong amylopectin chains (Hanashiro et al., 2008). Nomenclature of different chain categories of amylopectin as A, B, and C chains was established already in 1952, where A chains are unsubstituted, B chains are substituted with A chains or other B chains, and C chains carry the sole reducing end of the starch macromolecule and otherwise features similar to B chains (Peat et al., 1952).

The latest model used to explain the distribution of chains in amylopectin molecules is the building block backbone model, according to which the basic structural units of amylopectin are called building blocks (BB) (Bertoft, 2017; Tetlow & Bertoft, 2020). These BB spread out randomly from a backbone composed of a collective arrangement of long amylopectin chains (DP >36). Short amylopectin chains join the backbone to make branches, and also make connections with BB outside the backbone to form external BB. In some cases, these chains may remain as long branches to the backbone (Bertoft, 2017). The BB are made up of approximately 2–12 chains and, based on the number of chains, are grouped as G2 to G6. The G2 type consists of two chains (DP 5–9), G3 consists of three chains (DP 10–14), G4 has four chains (DP 15–19), G5 has on average six chains (DP 20–35), and G6 contains 9–12 chains (DP >35) (Bertoft et al., 2012; Tetlow & Bertoft, 2020).

Starch synthesis is a very complex biological process that involves many enzymes. The main enzymes involved in synthesizing amylose and amylopectin are starch synthases (SS), starch branching enzymes (SBE), and starch de-branching enzymes (DBE) (Tetlow & Bertoft, 2020). In potato, multiple isoforms of SS are present, which are differentiated

---

based on cDNA and amino acid sequence, i.e. granule bound starch synthase (GBSS), and soluble starch synthases (SSI, SSII, and SSIII), with each isoform having a distinct function in starch synthesis (Nazarian-Firouzabadi & Visser, 2017). GBSS is primarily responsible for amylose synthesis and is also possibly involved in amylopectin synthesis, particularly in the formation of the extra-long unit chain fraction (Nazarian-Firouzabadi & Visser, 2017). In general, SSI and SSII are responsible for synthesizing short to intermediate chains of amylopectin, while SSIII is proposed to synthesize long chains of amylopectin (Tetlow & Emes, 2011; Tetlow & Bertoft, 2020). Among the soluble isoforms of SS, SSIII is the major isoform in potato tubers, accounting for almost 80 % of soluble SS activity (Nazarian-Firouzabadi & Visser, 2017). SBEs attach branches on amylose and amylopectin molecules by cleaving an α-(1,4) bond within the α-glucan chain and transferring it to an α-glucan chain as an α-(1,6)-linked branch chain. There are two isoforms of SBE in potato, SBEI and SBEII, which differ in terms of substrate specificity and length of the α-glucan chains transferred. SBEI transfers amylose and long chains, while SBEII transfers relatively short (DP 6–14) α-glucan chains of amylopectin. DBEs are involved in trimming the amylopectin molecule and determining the final molecular structure of amylopectin (Tetlow & Bertoft, 2020).

Since starch is the main dry-weight component of potato tubers, its functionality is important for subsequent commercial applications of potato starch. New gene-editing technologies such as CRISPR/Cas9 are now being used as an efficient research tool to study gene functions and alter enzymatic pathways by inducing mutations in predefined genes or genetic elements. Altering the starch synthesis pathway by affecting starch synthesis enzymes, particularly SBE and GBSS, by CRISPR/Cas9 has proven to be effective in designing potato starch with distinctive molecular composition and structures to match specific end-uses (Andersson et al., 2017; Tuncel et al., 2019; Zhao et al., 2023; Zhao, Jayarathna, et al., 2021). A previous study by our research group showed that mutations in *SBE* genes generated by the CRISPR/Cas9 technique result in starch with altered chain length distribution and amylose content (Zhao, Jayarathna, et al., 2021). To advance this research further, we hypothesized that targeted mutations by CRISPR/Cas9 in *GBSS*, in addition to in *SBE* genes, would create starch with altered molecular and thermal properties, by altering amylose synthesis by *GBSS* mutagenesis. Therefore, the present study aimed to characterize starch generated through targeted mutations in *SBE* and/or *GBSS* induced using CRISPR/Cas9 technology, and to assess the relationship between molecular properties of the starch and its thermal properties. While conventional breeding techniques have been used in maize to generate or/and characterize amylose extender waxy homozygous genotype starch (Gérard et al., 2000; Yamada et al., 1978), to our knowledge the present study is the first to evaluate molecular properties of potato starch generated through mutations in both *GBSS* and *SBE* genes using CRISPR/Cas9 technology.

2. Materials and methods

2.1. Development of potato lines, greenhouse cultivation, and starch isolation

Mutations were induced in the *GBSS* gene in both a previously generated *SBEI-SBEII* mutational line 104018 (Zhao, Jayarathna, et al., 2021) and the wild-type cultivar Desiree, using PEG-mediated ribonucleoprotein (RNP) transfection of isolated protoplast. Plant tissue culture, protoplast isolation, transfection, regeneration, and mutation screening using high-resolution fragment analysis (HRFA) are described elsewhere (Andersson et al., 2018; Nicolia et al., 2021). The target region in *GBSS* is located in exon 8 of the gene, and a sgRNA, GT2, 5′-TGTTGACAAGGGTGTTGAAT−3′ was used to guide the Cas9 to the target site (Andersson et al., 2017). To confirm the HRFA results and analyze the distribution of mutated alleles, PCR amplification on extracted DNA from the separate event was performed using Phusion

polymerase (Thermo Fisher Scientific, Waltham, USA) with primers 5′-TCTCTGACTTCCCTCTTCTCA-3′ and 5′-GCAGCAACAAGAA-TATCTGAAC-3′ followed by Sanger sequencing (Eurofins Genomics, Ebersberg, Germany) and online ICE analysis (http://ice.synthego.com). Five lines with various *GBSS* mutations in the L6 background (L1-L5) and one *GBSS* knockout line (L7) were selected for further studies, together with their parental lines L6 and L8 (Table 1). Cuttings of the lines were planted in a greenhouse and grown between October 7 and January 22 under controlled conditions described elsewhere (Zhao, Jayarathna, et al., 2021). Starch was isolated from the harvested tubers as previously described (Larsson et al., 1996).

2.2. Determination of amylose content

Amylose content was determined on isolated starch fractions, after precipitating the amylopectin fraction, using Concanavalin A according to the assay protocol for the amylose/amylopectin kit (Megazyme, Wicklow, Ireland). All analyses were performed in duplicate and results are presented as mean of duplicates.

2.3. Microscopic analysis of starch granules

Purified starch was stained with Lugol's solution (109261, Merck KGaA, Darmstadt, Germany), diluted 1:1:1 with water and glycerol, and visualized by light microscopy (LeicaDMLB, Leica Microsystems, Wetzlar, Germany) with an assembled camera (Leica DFC450C, Leica Microsystems, Wetzlar, Germany). Polarized light microscopic analysis was performed for starch dispersions as described previously (Zhao, Jayarathna, et al., 2021). Starch dispersions of 50 mg/mL were prepared in distilled water and used to capture images with a 20× objective lens under polarized light. A light microscope (Leica DMLB, Wetzlar, Germany) equipped with an infinity X-32 digital camera (DeltaPix, Samourn, Denmark) was used for this purpose.

2.4. Wide angle X-ray diffraction analysis

The crystalline pattern and crystallinity of starch samples were determined by wide-angle X-ray diffraction analysis with Panalytical X'pert Pro. The powder diffractometer was operated at 45 kV and 40 mA, emitting Cu-Kα radiation at wavelength 1.54 Å. Diffraction patterns for duplicate samples were recorded between 5 and 40° 2θ. The degree of crystallinity (CI) was calculated based on the X-ray diffraction diagrams, according to a method described previously (Dome et al., 2020; Liu et al., 2009). A smooth line connecting the minimum diffraction intensities of the X-ray diffractogram was fitted, and the area under the smooth line was considered as the crystalline region. A straight line to connect the total area of 5–40° 2θ was also fitted. The area between the smooth line and the straight line was taken to represent the amorphous region. Then CI was calculated as the ratio between the crystalline area and the total area above the straight line (which represented both crystalline and amorphous areas).

2.5. Starch structural analysis

Chain length distribution pattern of de-branched starch and BB distribution in whole starch samples were studied. For determination of chain length distribution pattern, the starch samples were solubilized in UDMSO (0.6 M urea in 90 % DMSO), de-branched using isoamylase from *Pseudomonas* sp. (EC 3.2.1.68, 500 U/mL, Megazyme, Wicklow, Ireland) and pullulanase M1 from *Klebsiella planticola* (EC 3.2.1.41, 700 U/mL, Megazyme, Wicklow, Ireland), and studied using high-performance size exclusion chromatography (HPSEC) and high-performance anion exchange chromatography (HPAEC). The enzymes were de-salted through PD-10 desalting columns (Sephadex, Amersham Pharmacia Biotech AB, Uppsala, Sweden), and 10-fold diluted using acetate buffer (0.01 M, pH 5.0) prior to use. For HPSEC, 300 μL of each ten-fold diluted enzyme (15

Table 1

Size of induced mutations in potato genes *GBSS*, *SBEI*, and *SBEII*. "-" represents deletion, "+" represents insert, and "0" represents wild-type allele. Lines with a "0" have one wild type allele. The lacking indel in *SBE II* means two alleles have the same size of indel.

Line	Breeder's identification	Genetic background	Descriptive sample ID	GBSS (size of indels)	SBEI (size of indels)	SBEII (size of indels)
L1	150172	104018	gbss-IF1	−3;−2;−2;+1	−93;−23;−17;+153	−1;0;+104
L2	150183	104018	gbss -IF2	−37;−7;−5;−3	−93;−23;−17;+153	−1;0;+104
L3	150154	104018	gbss -KO1	−5;−4;−2;+1	−93;−23;−17;+153	−1;0;+104
L4	150068	104018	gbss -KO2	−5;−5;−1;−1	−93;−23;−17;+153	−1;0;+104
L5	150207	104018	gbss -WTIF	−19;−4;−3;0	−93;−23;−17;+153	−1;0;+104
L6	104018	Parental line	GBSS-NA		−93;−23;−17;+153	−1;0;+104
L7	149108	Desiree	gbss	−2;−1;+1;+1		
L8	Desiree	Wild type	WT			

Descriptive IDs were assigned based on GBSS mutations using the following rationale: gbss -IF (one in-frame allele), gbss -KO (four alleles with out-of-frame mutations), gbss -WTIF (one wild-type allele, one in-frame allele), GBSS-NA (no mutations for GBSS), gbss (only GBSS mutated), WT (wild-type variety). The last digits (1 and 2) of the descriptive IDs for L1-L4 indicate indel size variations between samples. Note: *SBEI* and *SBEII*mutations are consistent in samples L1-L6.

and 21 U respectively from isoamylase and pullulanase) and 400 μL of acetate buffer (0.01 M, pH 5.0) were mixed with 500 μL of solubilized starch sample for debranching overnight at 40 °C, followed by 10 min of boiling to terminate the enzyme reaction and filtration through a 0.45 μm nylon filter. Final starch concentration of the de-branching mixture was 3 mg/mL. For HPAEC, a five-fold diluted sample preparation from HPSEC was used. The HPSEC was equipped with two serially connected OHpak SB-802.5 HQ columns with a guard column (Shodex, Showa Denko KK, Miniato, Japan) kept at 35 °C. The eluent was 0.1 M NaNO$_3$ containing 0.02 % NaN$_3$, with a flow rate of 0.5 mL/min. The HPSEC was equipped with a refractive index (RI) detector (Shodex RI-501, Showa Denko KK, Miniato, Japan) and a multiple-angle laser light scattering detector (Wyatt Technology Corp., Santa Barbara, CA). The HPAEC setting and the program were explained by (Zhao, Jayarathna, et al., 2021).

For BB distribution analysis, the BBs were prepared as described by (Zhao, Andersson, & Andersson, 2021) using β-amylase (*E*-BARBL, Megazyme, Wicklow, Ireland) and α-amylase (E-BAASS, Megazyme, Wicklow, Ireland). β-amylase was used to remove the linear external chains of amylose and amylopectin, yielding β-limit dextrins (β-LDs). The β-LDs were then hydrolyzed with α-amylase to produce α-limit dextrins (α-LDs), which were treated with β-amylase to remove any remnants of external chains in the resulting BB. The enzymes were then denatured by heating in a boiling water bath, filtered through a membrane filter (0.45 μm) to isolate the BB, and used for further analysis as described previously (Zhao, Andersson, & Andersson, 2021). Both β-amylase and α-amylase were previously de-salted and diluted as described above.

The BB distribution was studied using HPSEC, with the same settings as described for de-branched chain length distribution pattern analysis.

ASTRA software (version 8.1.2, Wyatt Technology Corp., Santa Barbara, CA) was employed for data analysis of both the chain length distribution pattern of de-branched starch and BB distribution pattern. The presented results represent the mean of two replicates as obtained by RI detector, with the sample blank subtracted to eliminate enzyme and buffer peaks in the elution profiles. For chain length distribution of de-branched starch analysis, the chromatograms were normalized for peak area between 25 and 32 elution minutes and subsequently divided into 4 buckets for further analysis as fractions eluting between 25-26, 26–27, 27–29, and 29–32 min. The BB distribution pattern was normalized between 25 and 34 elution minutes and devided in to five groups (G2-G6) as G6: 25.0–26.4, G5: 26.4–27.9, G4: 27.9–29.9, G3: 29.9–31.3, and G2: 31.3–34.3 min for further analysis.

2.6. Analysis of thermal properties

Gelatinization and retrogradation properties of starch were studied using differential scanning calorimetry (DSC) with a DSC250 device (TA Instruments, New Castle, DE, USA) calibrated with indium. Gelatinization onset, peak, and end set temperatures were studied as described

previously(Zhao et al., 2023). Retrogradation properties were studied for crystal melting onset and peak temperatures of retrograded starch. First, 25 mg of starch were cooked with 50 μL of water at 121 °C for 15 min in sealed high-volume stainless-steel pans in an autoclave-steam sterilizer (Model 2840ELCG-D, Tuttnauer, The Netherlands), to ensure gelatinization of all starch. The gelatinized starches were then stored at 5 °C for three days prior to analysis.

2.7. Statistical analysis

Differences in measured parameters were studied by one-way analysis of variance (ANOVA). Tukey pairwise comparisons, Dunnett's test and Pearson correlation coefficient analysis were performed at confidence level 95 % ($p < 0.05$) using Minitab 21 (State College, PA, USA).

3. Results and discussion

3.1. Mutagenesis of GBSS for stacking mutations

Mutations in *GBSS* were induced in potato line 104018, a previously generated *SBEI* and *SBEII* mutational line of the potato cultivar Desiree that has all four alleles of *SBEI* mutated, while *SBEII* has at least one wild-type allele remaining (Zhao, Jayarathna, et al., 2021). The selected stacked lines with additionally induced mutations in *GBSS* resulted in: i) four allele mutational lines having one allele with an in-frame mutation (L1,L2); ii) all four alleles of GBSS having out-of-frame mutations (L3, L4); and iii) mutations in three of four alleles (L5) (Table 1). Additionally, one line (L7) with mutations induced only in *GBSS*, with four alleles with out-of-frame mutations, was generated in the Desiree (L8) background (Table 1). CRISPR/Cas9 targets were directed to coding regions of the genes, which means that it is not the expression of the genes per se that is affected but rather the structure of the resulting protein. Out-of-frame mutations will result in a disrupted protein primary structure downstream of the target site while in-frame mutations will result in the loss of one or more amino acids while the rest of the protein will remain as wild type regarding primary protein structure.

3.2. Amylose content

The amylose content, determined through the complex formation between Concanavalin A and amylopectin using an amylose/amylo-pectin determination kit (Megazyme, Wicklow, Co, Ireland), is depicted in Fig. 1.The highest amylose content was observed for line L5 (49%), followed by L6 (38%). The waxy potato line L7 had the lowest amylose content (3 %). The amylose content of the wild-type L8 was 27 %.

The high amylose content in L6 was attributed to the mutations in the *SBEs*. As elucidated by Zhong et al. (2022, 2023), high-amylose starches are frequently generated by inhibiting pivotal enzymes in the amylopectin biosynthesis pathway, resulting in a decrease in the amylopectin proportion and an increase in the amylose proportion. In
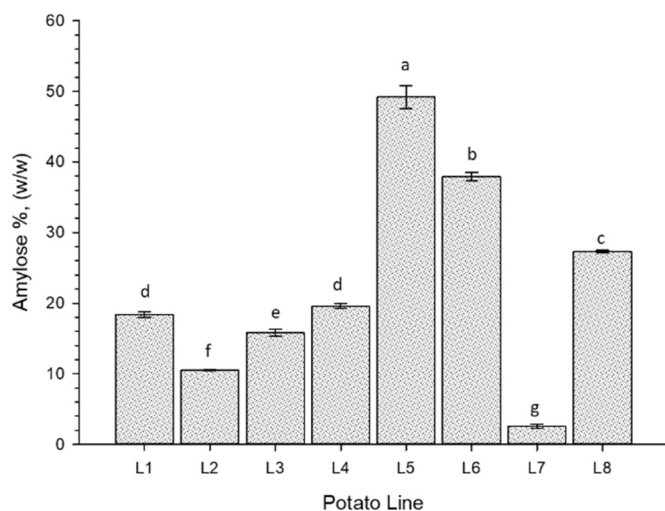
Fig. 1. Amylose content of starches from potato lines L1-L8 measured based on complex formation between Concanavalin A and amylopectin. Values shown are the mean of two technical replicates, error bars indicate standard deviation, and different letters on bars indicate statistically significant differences as analyzed by Turkey comparison (p < 0.05). L1: gbss -IF1, L2: gbss -IF2, L3: gbss -KO1, L4: gbss -KO2, L5: gbss -WTIF, L6:GBSS-NA, L7: gbss, L8:WT.

addition to the enhancement of amylose content through the inhibition of amylopectin biosynthesis, it is highly probable that these inhibitions also exert an influence on the structural composition of the amylopectin chains. High amylose or amylose-only starch in crops with down-regulated or mutated *SBEs* has been reported previously for both cereal and tuber starches (Carciofi et al., 2012; Huang et al., 2015; Li et al., 2019; Zhao et al., 2018; Zhao, Jayarathna, et al., 2021). Therefore, high amylose feature of starch in *SBE*-suppressed crops can have two explanations. First, suppressing the activity of SBE could reduce the amount of amylopectin, thereby increasing the relative proportion of amylose. Second, suppression of SBE activity could reduce the frequency of branching of amylopectin, inhibiting the introduction of α-1,6-linkages into starch and promoting formation of long amylose-like chains of amylopectin (Seung, 2020; Zhong et al., 2022, 2023).

The method of amylose determination using Concanavalin A is based on the principle described by Yun and Matheson (1990). Amylopectin was first precipitated with lectin Concanavalin A as a complex, and the supernatant containing amylose was enzymically hydrolyzed to D-glucose and analyzed using glucose oxidase/peroxidase reagent. As described by Matheson and Welsh (1988), Concanavalin A forms complexes with glucan polymers through interacting with the non-reducing ends of glucan polymers. These interactions and associations are less frequent with amylose, since it has much fewer non-reducing ends than amylopectin. Therefore, the molecular structure of these glucan polymers plays a crucial role in determining complex formation with Concanavalin A. Considering the method of determination, amylopectin with altered molecular structure with more long chains with fewer branches runs a risk of not complexing with Concanavalin A and ending up in the supernatant, where it can later be detected as amylose.

The high amylose content identified in line L5 may be attributed to the existence of a wild-type allele in the *GBSS* gene. Consequently, amylose production could occur nearly as normal, given the residual activity of the GBSS enzyme. This suggests that presence of only one wild-type allele is enough for reaching almost the same level of GBSS enzyme as in native potatoes. Besides the amylose produced by the GBSS enzyme, mutations in *SBE* genes, which inhibit the branching of amylopectin, may also contribute to the total amylose content of line L5. An interesting observation was that L5 exhibited a higher amylose content (49 %) compared to L6 (38%), even with mutations induced in three out of four *GBSS* alleles in L6. This could suggest an altered activity

of other enzymes, besides GBSS, building long chains in an *SBE* suppressed background. Furthermore, additional factors, such as the downregulation of amylopectin production enzymes, may impact the ratio between amylose and amylopectin. These factors could play a role in determining amylose content independently of the activity of the GBSS enzyme. A deeper study of L5 is needed to elucidate the mechanisms behind this effect.

All other lines (L1-L4) had a lower amylose content than L6, which can be linked to the mutations in the *GBSS* gene. However, even with complete knockout of the *GBSS* gene, L3 and L4 still had an amylose content of 20 % and 16 %, respectively. This indicates probable compensation for the role of GBSS by other active enzymes in starch synthesis when *GBSS* is simultaneously mutated in an *SBE*-suppressed background, or synergetic effects of different starch biosynthetic enzyme isoforms. Synergy between different isoforms of SS and SBE has been discussed previously, e.g., the substrate for a particular isoform might be the product of another (Smith, 1999). Altered expression of one isoform might then cause alteration in the substrate for another isoform, which might lead to production of structures that are abnormal (i.e., amylose-like glucan chains in a *GBSS*-knocked out *SBE* mutated background). The amylose content of *GBSS*-knocked out lines L3-L4 lines might also be attributable to the function of SSIII in an *SBE*-suppressed background. It is proposed that SSIII synthesizes long amylopectin chains (Tetlow & Emes, 2011; Tetlow & Bertoft, 2020) but in an *SBE* mutated background these chains will have lower branching frequency with fewer non-reducing ends to make complexes with Concanavallin A, and will be detected later as amylose. Further experiments are needed to confirm this.

When only *GBSS* is mutated, without suppressing the *SBEs*, the plant can no longer produce amylose and this results in waxy phenotypes such as line L7. In a previous study where mutations were induced in all four alleles of *GBSS* using the CRISPR/Cas9 technique, two different methods were used to measure the amylose content, which was found to be 0 % when determined by the perchloric acid method and 4.4 % based on the Megazyme kit method (Toinga-Villafuerte et al., 2022).

3.3. Starch granule morphology

Iodine staining of non-waxy and waxy starches showed specific blue-black and red-brown color, respectively (Seguchi et al., 2000), attributable to the presence or absence of apparent amylose. In agreement, lines L5, L6, and L8, with normal or high amylose content, stained blue, the *GBSS* knockout line (L7) stained pale red-brown, and the low-amylose lines L1 and L2 with in-frame mutations in *GBSS* stained pale purple (Fig. 2). However, starch from lines L3 and L4, with *GBSS* fully knocked out and *SBE* mutated, also stained pale purple, although some granules of L3 stained dark blue at the hilum (Fig. 2). Iodine staining of granules from *GBSS* knockouts, particularly in an *SBE* mutated background, could be attributable to the affinity of iodine to long amylopectin chains with reduced branching frequency. It could also be partly explained by starch granule formation starting from the hilum (Seung & Smith, 2019) and by *SSIII* synthesizing long amylopectin chains (Tetlow & Bertoft, 2020; Tetlow & Emes, 2011) which, with reduced branching frequency in an *SBE* mutated background, might show affinity to iodine complexation. It has been shown that *SSIII* may play a role in starch granule initiation in *Arabidopsis* (Szydlowski et al., 2009), and may also do so in potato tuber starch.

Under the light microscope, the iodine-stained starch revealed significant differences in granule morphology between the different potato lines (Fig. 2). Alterations in potato starch granule morphology as affected by Cas9-mediated mutagenesis in genes involved in starch synthesis has been observed previously (Tuncel et al., 2019; Zhao, Jayarathna, et al., 2021). The potato line L6 (parent to L1-L5), with mutations in only the *SBE* genes, had a highly altered granule phenotype compared with native potato starch, e.g., the starch granules were more irregular in shape and had rough surfaces (Fig. 2). Irregular shape of
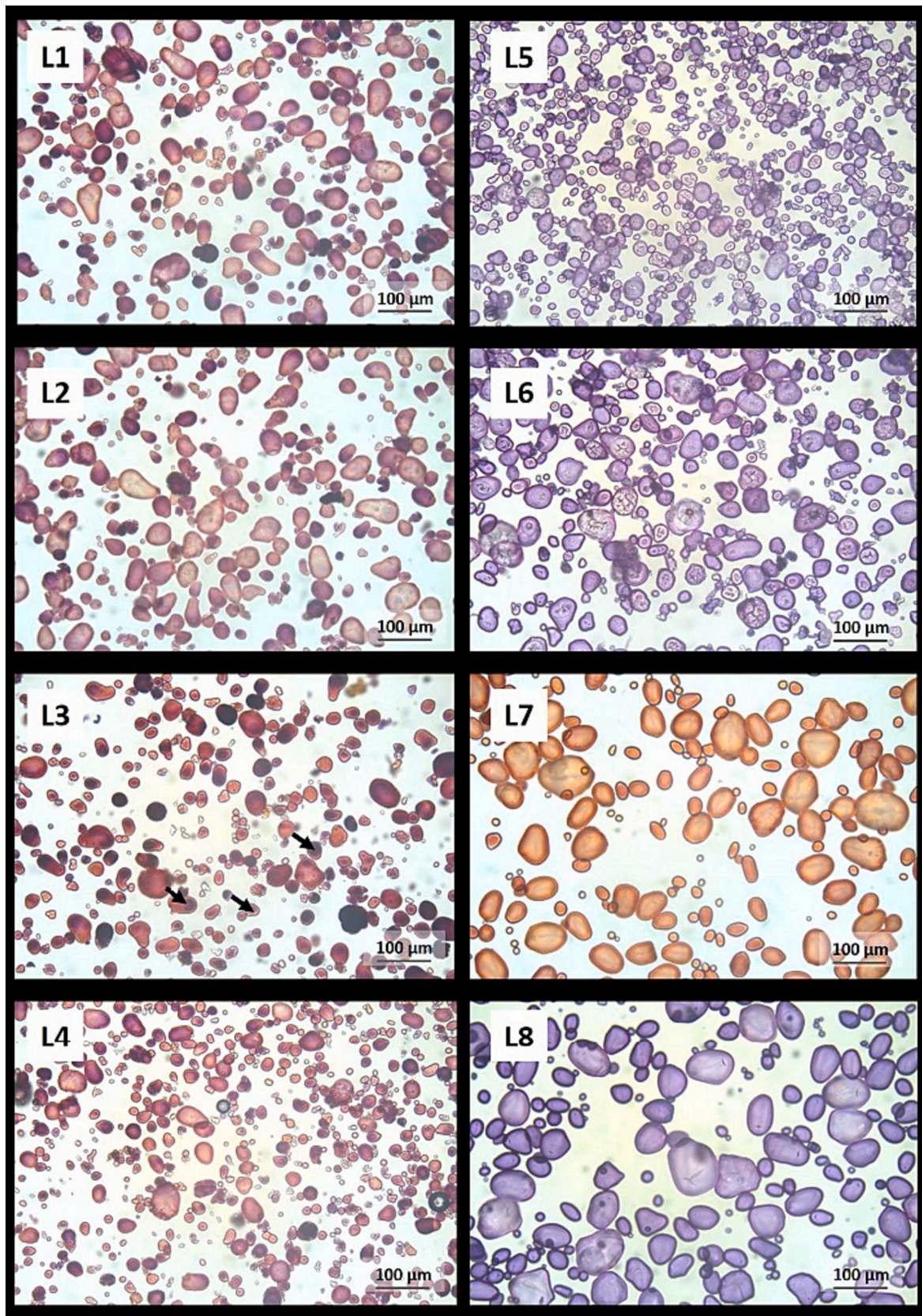
Fig. 2. Morphology of starch granules in potato lines L1-L8 stained with iodine and visualized under light microscope. Black arrows in L3 indicate the stained hilum area in dark blue. L1: gbss -IF1, L2: gbss -IF2, L3: gbss -KO1, L4: gbss -KO2, L5: gbss -WTIF, L6:GBSS-NA, L7: gbss, L8:WT.

starch granules in L6, but in a different greenhouse cultivation period, was observed in our previous study (Zhao, Jayarathna, et al., 2021). Interestingly, introducing mutations in *GBSS*, in addition to the *SBE* genes, restored the granule phenotype to a considerable extent in lines L1- L4, generating granules with nearly oval shapes and smooth surfaces (Fig. 2). However, L5 had similar granule morphology to the parental line L6, most likely owing to presence of an unmutated *GBSS* allele in L5. The GBSS enzyme is usually present in surplus and the presence of an unmutated allele in the *GBSS* gene might be sufficient to produce starch granules with similar morphology to those in *GBSS* unmutated potato line L6. As seen in a previous study (Zhao, Jayarathna, et al., 2021), mutations in *SBEs* alter starch granule morphology significantly. However, starch granule morphology is reported not to be affected by knocking down the *GBSS* gene (Brummell et al., 2015), as observed here for granule morphology of the *GBSS*-knocked out line L7. However, in the present study stacking mutations in *GBSS* in an *SBE*-mutated background was able to restore starch granule morphology somewhat (in L1-L4), which could be due to the individual effect of mutations of *GBSS* or a combined effect of the mutations.

3.4. Polarized light microscopy

In general, most starch granules show Maltese cross birefringence pattern when studied under polarized light microscope which indicate a radial arrangement of crystallites (Pérez et al., 2009) In agreement, all starches studied under the polarized light microscope showed Maltese crosses but with differences in appearance (Fig. 3). Starch granules from the wild-type potato (L8) showed very clear Maltese cross birefringence patterns, as reported previously for native potato starches (Tuncel et al., 2019; Zhao, Jayarathna, et al., 2021). Waxy potato starch (L7) showed similar Maltese crosses to L8, while L5 and the parental line L6 did not show clear Maltese crosses at the center of the granules (Fig. 3). As explained by French (1984), the intensity of birefringence appears to depend on the granule thickness, crystallinity and orientation of the crystallites. Hence, the reduced intensity of Maltese crosses observed in the starch from L5 and L6 may be ascribed to alteration of any of the aforementioned factors.

3.5. X-ray diffraction pattern and degree of crystallinity

As expected for tuber starch, starch from all potato lines displayed a B-type X-ray diffraction pattern (Fig. 4), with main peaks at 15° (broad), and 17° (strong), and a doublet at 22–24° for 2θ (Zhao et al., 2018; Zhao, Jayarathna, et al., 2021). Therefore, none of the targeted mutations altered the crystalline pattern of the starches. However, variations in CI were observed (Table 2). According to previous studies, the CI of native potato starch is around 20–25 % (dos Santos et al., 2016), while the total crystallinity of waxy potato starch is 30.01 ± 0.11 % (Jiranuntakul et al., 2011). The CI values obtained in the present study were close to previously reported values. Dunnett's multiple comparison, taking L8 as the control sample, revealed that potato starches from lines L2, L5, and L7 grouped with L8, with lower CI than starch from the other lines. Among those lines with a lower CI, line L5 displayed the lowest CI value (24.6 %), which could be due to the large increase in amylose content lowering the relative content of amylopectin, the fraction responsible for the crystallinity of starch granules.

3.6. Chain length distribution of debranched starch

HPSEC and HPAEC were used to investigate the chain-length distribution pattern of de-branched starches. In the HPSEC chromatogram (Fig. 5a), the fraction eluting after 25 min is associated with chains originating from the amylopectin molecules, while the peaks eluting before 25 min are associated with chains from amylose molecules. Based on the HPSEC results, all mutant potato lines (L1-L6) showed substantially different chain length distribution pattern compared with the

wild-type L8 for both amylose and amylopectin fractions, while the amylopectin fraction in the *GBSS*-knockout L7 was similar to that in L8 (Fig. 5a). On comparing the chain length distribution patterns of lines with mutations in both *SBEs* and *GBSS* (L1-L5) with that of their parental line with mutations only in *SBEs* (L6), substantial changes to the amylose fraction were observed. Long chains eluting between 22 and 23 min were observed only for L8, L6, and L5 (Fig. 5a). This could be attributed to a certain chain category of amylose. The same lines all stained blue in color with iodine (Fig. 2), which indicates that molecules eluting at 22–23 min were responsible for the color shift in iodine from red-brownish to blue in those samples. An interesting observation was a peak of around 24 min in all the samples. Compared with the wild-type L8 and *GBSS* mutated L7, the 24- min peak was more prominent in all lines with *SBE* mutations. In a previous study, we also observed a prominent peak of such amylose component in *SBE* mutated lines compared with a wild-type line (Zhao, Jayarathna, et al., 2021). Comparing the chain length distribution to the granule phenotype and coloring from the iodine staining (Fig. 2), the molecules eluting in this region were likely responsible for the pale purple staining in *GBSS*-knocked out lines in an *SBE* mutated background. Taking into account the prominent peak observed approximately at 24 min in *SBE* mutated lines, coupled with the diminished iodine binding capacity of the constituent eluting at around 24 min, it may also be recognized as a constituent of high-amylose starch formed due to restrained SBE activity. This phenomenon has been denoted as amylose-like material, as explicated by Zhong et al. (2022). Further, lines L4 and L3 had a similar amylose chain length distribution pattern, as did lines L1 and L2. From this observation, it can be concluded that the chain length distribution pattern of the amylose fraction in potato starch is determined systematically and may be related to the type of mutation.

However, the chain distribution pattern of the amylopectin fraction in lines L1-L5 was mostly closer to that of L6 for all lines except for L5. This suggests that activity of the intact wild-type allele of *GBSS* in L5 not only increased the proportion of amylose in starch but also had a small effect on the molecular structure of amylose and amylopectin polyglucans in an *SBE* mutated background. A contribution of GBSS enzyme activity in determining amylopectin molecular structure has been reported previously (Brummell et al., 2015), with authors suggesting that reduced activity of GBSS may have some small effects on amylopectin structure, besides enhanced amylopectin content of potato starch.

The molar proportion distribution of starch from different potato lines, analyzed by HPAEC, is shown in Fig. 5b. In agreement with previous findings (Zhao, Jayarathna, et al., 2021), starch from L8 showed a dominant broad peak of amylopectin chains spanning DP ~9–33, but with a shift in the highest molar proportion of chains to DP 13 instead of DP 11. The Waxy L7 line, with mutations only in *GBSS*, had a very similar chain length distribution pattern of the amylopectin fraction as L8. All other lines showed substantial differences in amylopectin chain length distribution pattern compared with L8.

Differences in the abundance of different categories of amylopectin unit chains in the different lines were apparent from both the HPSEC and HPAEC results (Table 3). Interestingly, high-amylose line L5 showed the highest abundance of the longest amylopectin fractions (fractions eluting between 25 and 26 min and 26–27 min in HPSEC analysis, B2 and B3 chains in HPAEC analysis) and the lowest abundance of short amylopectin fractions (fractions eluting between 27 and 29 min and 29–32 min in HPSEC analysis, A chains in HPAEC analysis). Therefore, L5 revealed a very interesting starch type with high amylose content and long amylopectin chains.

Tukey pairwise comparisons for the normalized amylopectin fraction eluted between 25 and 32 min in HPSEC analysis revealed no difference in abundance or distribution pattern of amylopectin chain fractions between L8 and waxy L7. Therefore, knocking out only the *GBSS* gene did not affect the distribution pattern or abundance of different categories of amylopectin fractions. This observation was further supported by Tukey pairwise comparisons of the different chain categories for the
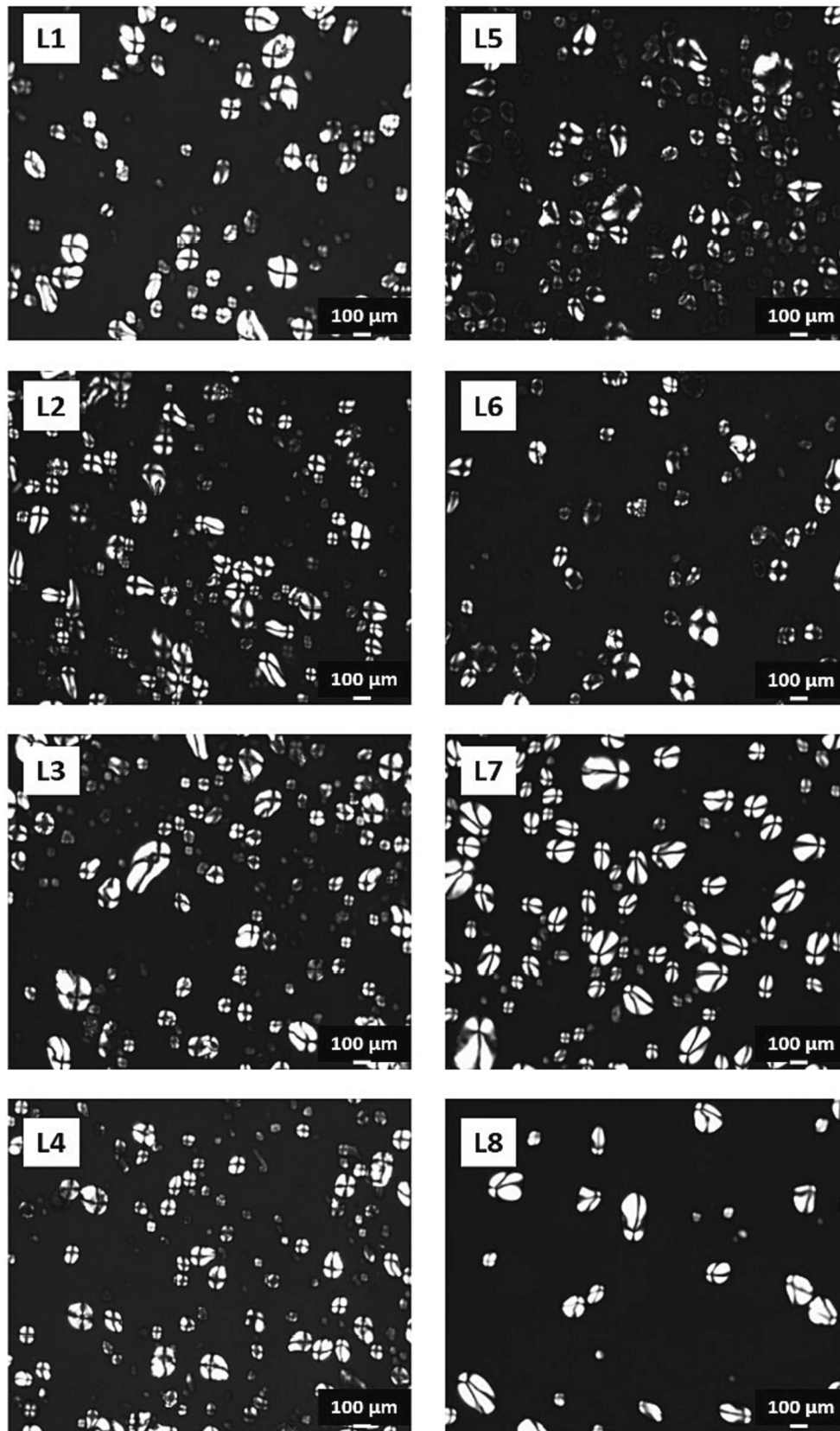
Fig. 3. Polarized light microscopy images of potato lines L1-L8. L1: gbss -IF1, L2: gbss -IF2, L3: gbss -KO1, L4: gbss -KO2, L5: gbss -WTIF, L6:GBSS-NA, L7: gbss, L8:WT.
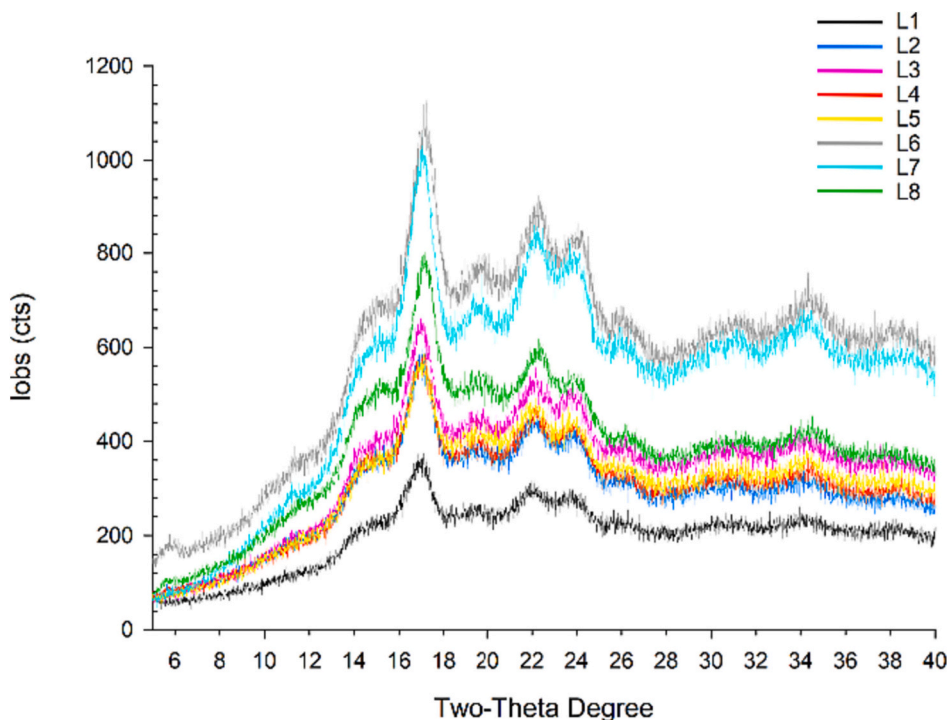
Fig. 4. X-ray diffraction patterns of starches from the experimental potato lines L1-L7 and reference variety L8. Diffraction intensity values are the mean of two replicates. L1: gbss -IF1, L2: gbss -IF2, L3: gbss -KO1, L4: gbss -KO2, L5: gbss -WTIF, L6:GBSS-NA, L7: gbss, L8:WT.

Table 2
Crystallinity degree (CI, %) of starches from potato lines L1-L8. L1: gbss -IF1, L2: gbss -IF2, L3: gbss -KO1, L4: gbss -KO2, L5: gbss -WTIF, L6:GBSS-NA, L7: gbss, L8:WT.

Potato line	CI %
L1	34.4 ± 0.1
L2	29.7 ± 2.3
L3	32.5 ± 2.1
L4	31.3 ± 0.3
L5	24.6 ± 0.4
L6	30.6 ± 0.7
L7	28.7 ± 0.1
L8	26.1 ± 1.7

molar proportion distributions in HPAEC analysis (Table 3). Similar chain length distribution of the short amylopectin fraction (up to DP 35) between a wild-type potato line and *GBSS* antisense lines has been reported previously (Fulton et al., 2002).

However, differences in the abundance of different amylopectin unit chain categories compared with L8 were observed in many of the lines evaluated in the present study, indicating that simultaneous mutations in *GBSS* together with *SBE* genes could result in starch with altered structure in the amylopectin fraction. It is of interest to note the influence of the *GBSS* gene in determining amylopectin molecular structure in an *SBE* mutated background.

Further, Pearson correlation analysis revealed a positive correlation between amylose content and B3 chains of amylopectin. Positive correlations between long amylopectin chains and amylose content have been reported previously for other types of starches (Lin et al., 2022; Wang et al., 2018). As reviewed by Wang et al. (2017), and as mentioned previously in this paper, crops deficient in SBE activity not only tend to produce more amylose, but also produce amylopectin enriched with long branches. This might be the reason for the positive correlation between amylose content and B3 chains in the present study.

Dunnett multiple comparison of the HPSEC results for lines L1-L5,

taking parental L6 line as the control sample, revealed differences in the abundance of different amylopectin unit chains except for the peaks eluted at 27–29 min (data not shown). This could be explained by the fact that both molecular structure and relative amounts of glucan polymers are affected by the mutations. Individual variations in *GBSS* mutations in an *SBE* mutated background could have a significant impact on chain length distribution of the amylopectin fraction, where a remaining wild-type allele in *GBSS* (L5) could produce long amylopectin glucan chains in an *SBE* mutated background.

3.7. Starch internal structure at the building block level

The distribution of building blocks (BB) was studied using HPSEC. In the HPSEC chromatogram (Fig. 6), the BB distributions were divided into five groups (G6-G2) for further analysis. The chromatogram also included the linear dextrin produced during BB preparation. The BB distribution displayed two clear distribution patterns that were attributed to samples with and without mutations in the *SBE* genes. The Waxy L7 line, with only mutation in *GBSS*, had a similar BB distribution to wild-type L8. There were some individual variations in the abundance of different groups of BB, as shown in Table 4, which can be attributable to the type of mutations induced.

Mutations only in *GBSS* (potato line L7) had no influence in determining the size distribution of BB, which grouped with the wild-type L8. Mutations only in *SBEs* (line L6) caused alterations in the size distribution of BB compared with wild-type L8, proving that mutations in *SBE* play a significant role in starch fine structure at BB level (Table 4).

There was a trend for large (G6 and G5) and medium-sized (G4) BBs to be present in comparatively higher abundance in lines L1, L4, and L5, while the small BBs (G3 and G2) were least abundant in those lines. This is an interesting observation and indicates that BB size is determined in a systematic way. There were variations in some BB group categories between the lines with various *GBSS* mutations in the L6 background line (L1-L5) and the parental line L6 (Table 4). This provides the important insight that gene *GBSS* has an influence in determining the abundance of different size categories of BB in an *SBE* mutated
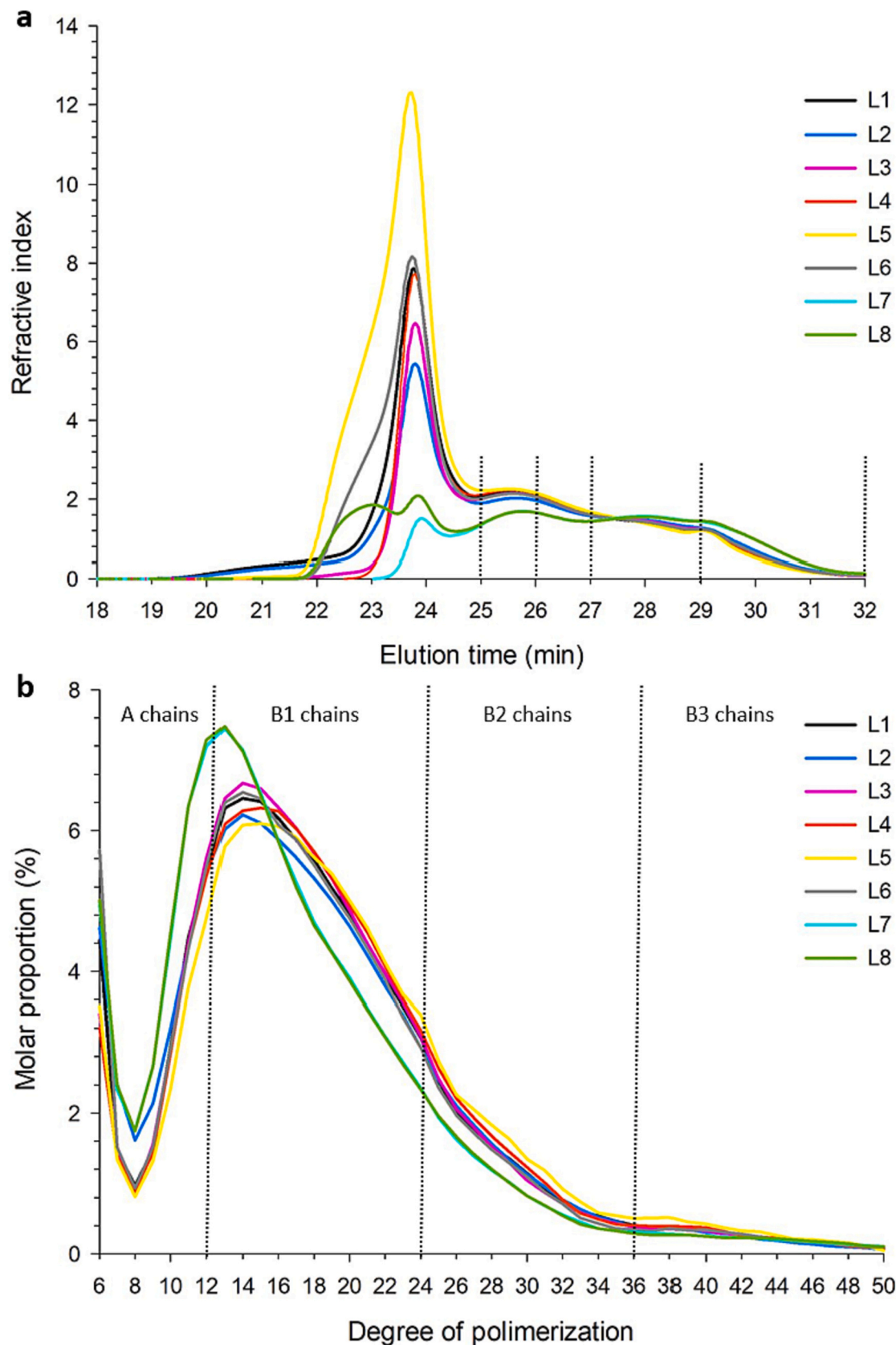
Fig. 5. Chain-length distribution of debranched starches from potato lines L1-L8, analyzed (a) by HPSEC on a relative weight basis after normalization for the amylopectin peak area (25–32 min), (b) by HPAEC on a relative molar basis with the degree of polymerization (DP) 6–50. In the HPSEC chromatogram (a), the amylopectin fraction eluted after 25 min is bucketed into several buckets marked by dash lines as fractions eluting between 25 and 26, 26–27, 27–29, and 29–32 min. In the HPAEC analysis (b), amylopectin chains were categorized according to Hanashiro et al. (1996) as A chains (DP 6–12), B1 chains (DP 13–24), B2 chains (DP 25–36), and B3 chains (DP ≥37). L1: gbss -IF1, L2: gbss -IF2, L3: gbss -KO1, L4: gbss -KO2, L5: gbss -WTIF, L6:GBSS-NA, L7: gbss, L8:WT.

Table 3

Abundance of amylopectin chain categories in potato lines L1-L8, analyzed by HPSEC and HPAEC. HPSEC categorization was based on elution minutes (as shown in Fig. 5a), presented as refractive index area on a relative weight basis. HPAEC analysis categorized amylopectin chains as indicated in Fig. 5 (B) and presented as molar proportions (%). Significantly different values within cells are denoted by different superscript letters (ANOVA, α = 0.05). L1: gbss -IF1, L2: gbss -IF2, L3: gbss -KO1, L4: gbss -KO2, L5: gbss -WTIF, L6:GBSS-NA, L7: gbss, L8:WT.

|	Amylopectin chain category							
	25.00–26.00 min		26.01–27.00 min		27.01–29.00 min		29.01–32.00 min	
HPSEC analysis	L5	274[a]	L5	232[a]	L7	367[a]	L8	254[a]
	L4	269[b]	L4	226[b]	L8	365[a]	L7	253 [a]
	L1	261[c]	L1	222[b]	L2	351[b]	L2	191[b]
	L3	258 [c]	L6	221[b]	L3	346[bc]	L6	179[bc]
	L6	258[c]	L3	220[b]	L6	342[bc]	L1	178[bc]
	L2	244[d]	L2	214[c]	L1	339[c]	L3	175[c]
	L7	196[e]	L8	184[d]	L4	338[c]	L4	168[cd]
	L8	196[e]	L7	184[d]	L5	336[c]	L5	157[d]
HPAEC analysis	B3 chains		B2 chains		B1 chains		A chains	
	L5	4.1[a]	L5	16.3[a]	L3	62.9[a]	L8	30.0[a]
	L4	3.4[b]	L4	14.8[ab]	L4	62.4[a]	L7	29.7[a]
	L6	3.2[b]	L2	14.1[ab]	L5	61.7[a]	L2	23.7[a]
	L1	3.2[b]	L1	13.9[ab]	L1	61.7[a]	L6	22.4[b]
	L3	3.2[b]	L3	13.7[b]	L6	61.2[a]	L1	21.2[b]
	L2	3.0[b]	L6	13.2[b]	L2	51.2[a]	L3	20.2[b]
	L7	2.9[b]	L8	10.7[c]	L7	56.8[a]	L4	19.5[b]
	L8	2.9[b]	L7	10.7[c]	L8	56.5[a]	L5	18.8[b]

background.

Pearson correlation analysis revealed an interesting correlation between different size categories of BB and different chain categories of amylopectin (HPAEC results) (Fig. 7). The large BB (G4, G5, and G6) showed a strong negative correlation with A chains, while the small BB (G2 and G3) showed a strong positive correlation. The large BB (G4, G5, G6) showed positive correlation with B1, B2, and B3 chains, while the smaller BB (G3, G2) showed a negative correlation.

Table 4

Variation in the normalized peak area of different size groups (G6-G2) of building block distributions in potato lines L1-L8. Values within columns with different superscript letters differ significantly (ANOVA, α = 0.05). L1: gbss -IF1, L2: gbss -IF2, L3: gbss -KO1, L4: gbss -KO2, L5: gbss -WTIF, L6:GBSS-NA, L7: gbss, L8:WT.

	Building block group				
Potato line	G6	G5	G4	G3	G2
L1	17.3[ab]	85.6[b]	356.7[b]	121.3[e]	419.1[d]
L2	12.1[c]	70.6[d]	320.1[d]	141.6[b]	455.6[b]
L3	14.4[bc]	79.3[c]	345.8[c]	128.5[c]	432.1[c]
L4	19.4[a]	90.7[a]	365.7[b]	120.6[d]	403.6[e]
L5	14.9[bc]	88.2[ab]	382.2[a]	112.2[e]	402.5[e]
L6	13.2[c]	79.1[c]	347.3[c]	132.1[c]	428.3[cd]
L7	2.1[d]	24.5[e]	189.3[e]	199.6[a]	584.5[a]
L8	2.9[d]	26.9[e]	195.5[e]	197.0[a]	577.7[a]
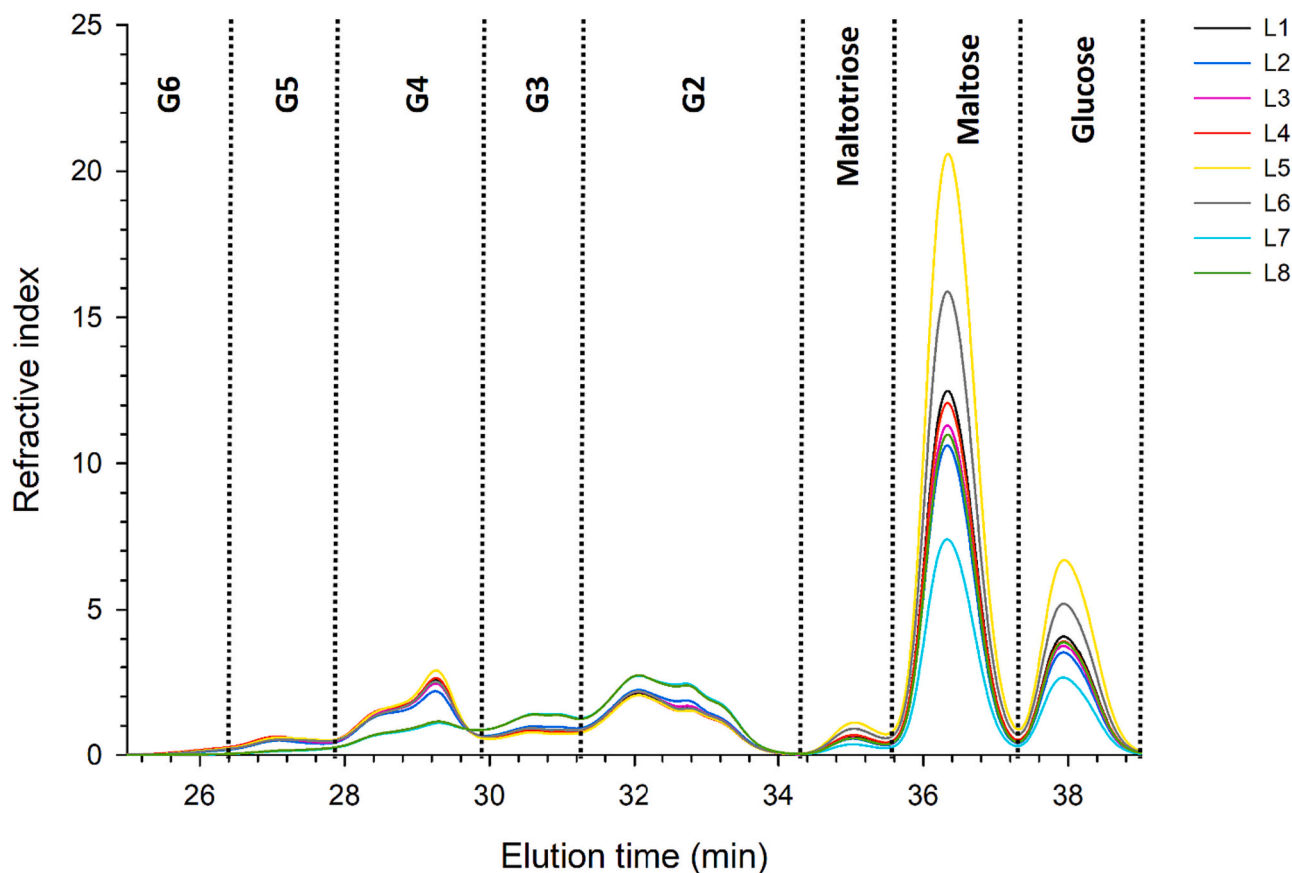
Fig. 6. Building block distribution in starch from potato lines L1-L8 after normalization for peak area, as determined by HPSEC. Normalization was performed for the area between 25 and 34 elution minutes. The distribution was bucketed in groups as G6: elution time 25.0–26.4, G5: 26.4–27.9, G4: 27.9–29.9, G3: 29.9–31.3, G2: 31.3–34.3 min. L1: gbss -IF1, L2: gbss -IF2, L3: gbss -KO1, L4: gbss -KO2, L5: gbss -WTIF, L6:GBSS-NA, L7: gbss, L8:WT.
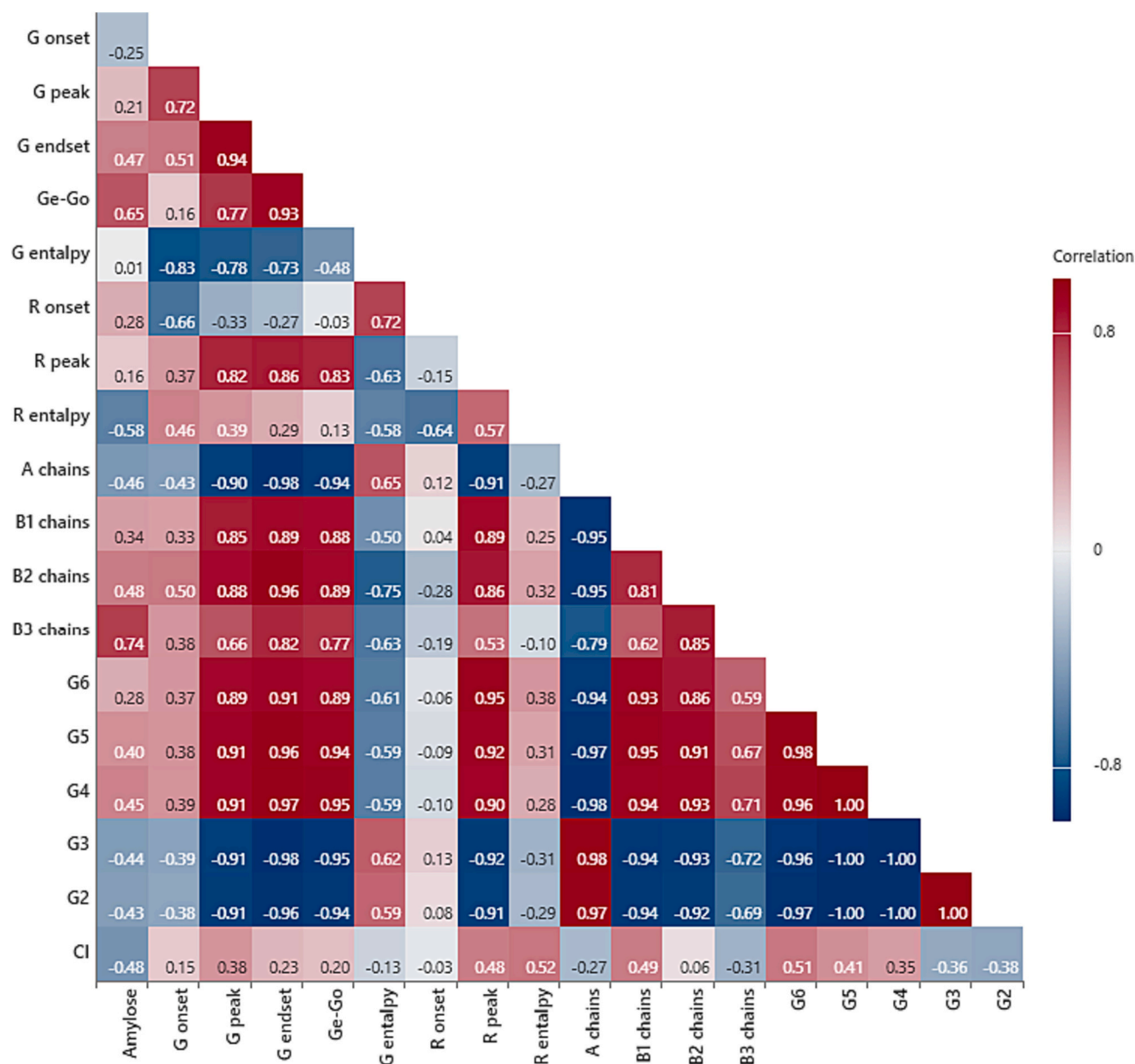
Fig. 7. Heat map of Pearson correlation results. G onset - gelatinization onset temperature, G peak - gelatinization peak temperature, G endset - gelatinization end set temperature, Ge-Go - gelatinization temperature range, R onset - retrogradation onset temperature, R peak - retrogradation peak temperature, R enthalpy- retrogradation enthalpy, A, B1, B2, B3 - amylopectin unit chains, G6-G2 - different size categories of building blocks, CI degree of crystallinity (%).

3.8. Thermal properties

3.8.1. Gelatinization properties

The gelatinization onset temperature (*To*) of starch from the different lines varied from 67.0 to 68.8 °C (Table 5). Line L8, with a higher proportion of shorter amylopectin chains (i.e., A chains from HPAEC analysis) showed the lowest *To*, peak temperature (*Tp*), and end set temperature (*Te*). Line L5, with the highest proportion of long chains (i.e., B2 and B3 chains from HPAEC analysis) showed the highest *To*, *Tp*, and *Te* values. This is in agreement with previous findings of low gelatinization temperature for samples with a high proportion of short amylopectin chains, and vice versa (Gomand et al., 2010). However, it is of interest to note that waxy line L7 also had high *To*, in agreement with previous findings of increases in potato starch *To* of around 4 °C when *GBSS* is silenced (Brummell et al., 2015). All the potato starches with mutations in *SBEs,* with or without mutation in *GBSS*, showed higher gelatinization temperatures than wild-type L8. This agrees with previous

Table 5
Gelatinization properties of starches from potato lines L1-L8. L1: gbss -IF1, L2: gbss -IF2, L3: gbss -KO1, L4: gbss -KO2, L5: gbss -WTIF, L6:GBSS-NA, L7: gbss, L8:WT.

Sample	*To* (°C)	*Tp* (°C)	*Te* (°C)	*Te-To* (°C)	*ΔH* J/g (amylopectin)
L1	67.5[c]	75.8[b]	85.3[b]	17.7[ab]	16.0[cd]
L2	68.4[b]	75.4[b]	83.4[b]	15.0[c]	16.7[cd]
L3	67.7[c]	75.3[b]	84.1[b]	16.4[bc]	17.8[bc]
L4	68.4[b]	76.9[a]	85.2[b]	16.8[bc]	16.0[cd]
L5	68.5[ab]	76.8[a]	87.8[a]	19.2[a]	15.1[d]
L6	67.0[d]	75.3[c]	84.0[b]	17.0[bc]	19.5[ab]
L7	68.8[a]	72.8[c]	78.7[c]	9.9[e]	17.4[bcd]
L8	64.8[e]	69.3[d]	77.4[c]	12.6[d]	20.7[a]

To - onset temperature, *Tp* - peak temperature, *Te* - end set temperature, *ΔH* - gelatinization enthalpy (calculated as J/g amylopectin). Values within columns with different superscript letters differ significantly (ANOVA, α = 0.05).

reports of a ∼ 5 °C increment in *Tp* of starch from potato tubers with low SBE activity (Safford et al., 1998). From Pearson correlation analysis (Fig. 7), it was apparent that *To*, *Tp*, and *Te* and the gelatinization temperature range (*Te-To*) had strong negative correlations with A chains and positive correlations with B1, B2, and B3 chains of the amylopectin fraction. As reviewed by Zhong et al. (2023), amylopectin with DP 6–12 (reffered as A chains in the present study) may introduce defects to the crystals, leading to the formation of starch granules with reduced gelatinization temperatures. This could potentially explain the observed negative correlation between A chains and gelatinization temperatures. Further, these gelatinization parameters were strongly positively correlated with large BB of G4, G5, and G6, and negatively correlated with small BB of G2 and G3, in agreement with (Zhao et al., 2023). A negative correlation between *Te* and A chains has been reported previously for maize starch (Lin et al., 2022). The gelatinization temperature range (*Te-To*) of waxy L7 was significantly lower ($p < 0.05$) than that of all other samples, possibly due to the fact that this line produced more uniform starch granules than the other samples. The fact that *Te-To* was highest for L5 may be due to the huge variation in granule morphology seen in the light microscopy images (Fig. 2).

Gelatinization enthalpy (*ΔH*) (corrected for amylopectin) was highest for wild-type L8, but with no significant difference compared with L6, which had the second highest *ΔH* value. In general, *ΔH* is an indicator of loss of molecular order within the granule, and gives an overall measure of quality and quantity of granule crystallinity. Introducing mutations might have negatively affected the molecular organization of starch granules, as represented by lower *ΔH* in all mutant lines than in L8. Pearson correlation analysis (Fig. 7) revealed a positive relationship of *ΔH* to A chains and a negative relationship to B chains. Even though both CI and crystal melting *ΔH* of starch are associated with the crystalline arrangement inside the starch granules, the trend in CI of starch samples from all lines except L5 did not follow the trend observed for *ΔH* of the starch samples. As discussed by Lourdin et al. (2015), it is not possible to use starch melting enthalpy to determine crystallinity, since numerous other processes such as plasticization, swelling in water, competition between melting, dissolution in water etc., are involved in melting. According to those authors, residual melting enthalpy should be used for relevant interpretations, but quantitative correlations with crystallinity cannot be made (Lourdin et al., 2015).

3.8.2. Retrogradation properties

Gelatinized starch undergoes a disorder-to-order transition defined as retrogradation. Starch retrogradation in lines L1-L8 was characterized by determining the Onset (*To*) and peak (*Tp*) temperatures of crystal melting and enthalpy change of retrograded starch gels (*ΔH*) after storage at 4 °C. However, an endothermic transition of retrograded starch reflects both melting of residual crystallites after gelatinization and recrystallized starch formed during retrogradation (Wang et al., 2016).

Table 6
Retrogradation properties of starches from potato lines L1-L8. L1: gbss -IF1, L2: gbss -IF2, L3: gbss -KO1, L4: gbss -KO2, L5: gbss -WTIF, L6:GBSS-NA, L7: gbss, L8:WT.

Sample	*To* (°C)	*Tp* (°C)	*ΔH* J/g (amylopectin)
L1	40.0[c]	74.0[ab]	10.6[ab]
L2	40.0[c]	73.0[ab]	11.0[a]
L3	42.5[ab]	74.2[ab]	10.2[abc]
L4	43.3[a]	75.0[a]	9.8[abc]
L5	40.3[bc]	73.2[ab]	9.3[abc]
L6	44.0[a]	70.8[bc]	8.4[c]
L7	40.3[bc]	67.3[d]	9.5[abc]
L8	44.0[a]	68.3[cd]	8.8[bc]

To - retrogradation onset temperature, *Tp* - retrogradation peak temperature, *ΔH* - retrogradation enthalpy. Values within columns with different superscript letters differ significantly (ANOVA, α = 0.05).

The highest *Tp* values were obtained for line L4, with no significant differences to lines L1, L2, L3 and L5 (Table 6). This is an interesting relationship of *Tp* to type of mutation where *Tp* raised by at least 5 °C in both *GBSS* and *SBE* mutated lines compared with L8. In Pearson correlation analysis (Fig. 7), a strong positive correlation of *Tp* with large BB (G4, G5, and G6) and a strong negative correlation with small BB (G2, G3) was observed. Correlations between BB size categories and retrogradation parameters have been reported previously (Zhao et al., 2023).

Retrogradation enthalpy (*ΔH*) was measured as enthalpy of the endotherm, and essentially reflected melting of ordered amylopectin. The highest *ΔH* value was obtained for L2, but it differed only from L8 and L6. There was an interesting trend for mutation in the *GBSS* gene to raise *ΔH* in the *GBSS* mutated lines (L1-L5, L7) compared with L8 and L6.

4. Conclusions

Mutations in *SBE* genes altered starch granule morphology from mostly oval-shaped, smooth granules to uneven granules with rough surfaces. However, stacking mutations in all four alleles of *GBSS* restored the granule phenotype to a considerable extent. Knocking out *GBSS* in an *SBE* mutated background decreased the measured amylose content (*w/w*) in starch from 38 % to around 20 %, while a waxy starch phenotype generated by individual knock-out of *GBSS* contained 3 % amylose. In addition to affecting amylose content, the enzyme GBSS played a role in determining the molecular structure of amylose in an *SBE* mutated background. Mutations only in *GBSS* had no significant impact in determining chain length and building block distribution pattern. However, mutations in *GBSS* influenced the abundance of different amylopectin unit chain categories and size distribution of whole starch building blocks in an *SBE* mutated background. The whole starch building block size categories were correlated with the abundance of different unit chains of amylopectin and with the thermal properties of the starch. The novel starch types, distinguished by their unique molecular and thermal properties, offer significant opportunities for application in both food and non-food domains. For example, L5, with its notable high amylose content and long amylopectin chains likely facilitate retrogradation and, shows promise as a potential resistant starch for healthier food components. Moreover, the increased gelatinization temperatures of *SBE* mutated lines could prove valuable in contexts favouring delayed gelatinization, while the increased retrogradation temperatures of *SBE* + *GBSS* mutated lines might be preferable in both food and non-food applications, enhancing sensory qualities and material properties, respectively. However, further studies are recommended to comprehensively explore the potential applications of these novel starch types.

CRediT authorship contribution statement

Shishanthi Jayarathna: Writing – review & editing, Writing – original draft, Visualization, Validation, Software, Methodology, Investigation, Formal analysis, Data curation, Conceptualization. **Per Hofvander:** Writing – review & editing, Methodology, Investigation, Funding acquisition, Data curation. **Zsuzsanna Péter-Szabó:** Writing – review & editing, Methodology, Investigation, Data curation. **Mariette Andersson:** Writing – review & editing, Supervision, Project administration, Methodology, Investigation, Funding acquisition, Formal analysis, Data curation, Conceptualization. **Roger Andersson:** Writing – review & editing, Supervision, Project administration, Funding acquisition, Conceptualization.

Declaration of competing interest

The authors declare that they have no known competing financial interests or personal relationships that could have appeared to influence the work reported in this paper.

Data availability statement

The original contributions presented in the study are included in the article, further inquiries can be directed to the corresponding author.

Acknowledgements

References

Andersson, M., Turesson, H., Nicolia, A., Fält, A.-S., Samuelsson, M., & Hofvander, P. (2017). Efficient targeted multiallelic mutagenesis in tetraploid potato (*Solanum tuberosum*) by transient CRISPR-Cas9 expression in protoplasts. *Plant Cell Reports, 36*, 117–128.

Andersson, M., Turesson, H., Olsson, N., Fält, A.-S., Ohlsson, P., Gonzalez, M. N., … Hofvander, P. (2018). Genome editing in potato via CRISPR-Cas9 ribonucleoprotein delivery. *Physiologia Plantarum, 164*, 378–384.

Bertoft, E. (2017). *Understanding starch Structure: Recent progress. Agronomy, 7*, 56.

Bertoft, E., & Blennow, A. (2016). Chapter 3—Structure of potato starch. In J. Singh, & L. Kaur (Eds.), *Advances in potato chemistry and technology* (2nd ed., pp. 57–73). San Diego: Academic Press.

Bertoft, E., Koch, K., & Åman, P. (2012). Structure of building blocks in amylopectins. *Carbohydrate Research, 361*, 105–113.

Brummell, D. A., Watson, L. M., Zhou, J., McKenzie, M. J., Hallett, I. C., Simmons, L., … Timmerman-Vaughan, G. M. (2015). Overexpression of starch branching enzyme II increases short-chain branching of amylopectin and alters the physicochemical properties of starch from potato tuber. *BMC Biotechnology, 15*, 28.

Carciofi, M., Blennow, A., Jensen, S. L., Shaik, S. S., Henriksen, A., Buléon, A., … Hebelstrup, K. H. (2012). Concerted suppression of all starch branching enzyme genes in barley produces amylose-only starch granules. *BMC Plant Biology, 12*, 223.

Dome, K., Podgorbunskikh, E., Bychkov, A., & Lomovsky, O. (2020). Changes in the crystallinity degree of starch having different types of crystal structure after mechanical pretreatment. *Polymers, 12*, 641.

dos Santos, T. P. R., Leonel, M., Garcia, É. L., do Carmo, E. L., & Franco, C. M. L. (2016). Crystallinity, thermal and pasting properties of starches from different potato cultivars grown in Brazil. *International Journal of Biological Macromolecules, 82*, 144–149.

French, D. (1984). Chapter vii - organization of starch granules. In R. L. Whistler, J. N. Bemiller, & E. F. Paschall (Eds.), *Starch: Chemistry and technology* (2nd ed., pp. 183–247). San Diego: Academic Press.

Fulton, D. C., Edwards, A., Pilling, E., Robinson, H. L., Fahy, B., Seale, R., … Smith, A. M. (2002). Role of granule-bound starch synthase in determination of amylopectin structure and starch granule morphology in potato. *Journal of Biological Chemistry, 277*, 10834–10841.

Gérard, C., Planchot, V., Colonna, P., & Bertoft, E. (2000). Relationship between branching density and crystalline structure of A- and B-type maize mutant starches. *Carbohydrate Research, 326*, 130.

Gomand, S. V., Lamberts, L., Derde, L. J., Goesaert, H., Vandeputte, G. E., Goderis, B., … Delcour, J. A. (2010). Structural properties and gelatinisation characteristics of potato and cassava starches and mutants thereof. *Food Hydrocolloids, 24*, 307–317.

Hanashiro, I., Abe, J., & Hizukuri, S. (1996). A periodic distribution of the chain length of amylopectin as revealed by high-performance anion-exchange chromatography. *Carbohydrate Research, 283*, 151–159.

Hanashiro, I., Itoh, K., Kuratomi, Y., Yamazaki, M., Igarashi, T., Matsugasako, J., & Takeda, Y. (2008). Granule-bound starch synthase I is responsible for biosynthesis of extra-long unit chains of amylopectin in Rice. *Plant and Cell Physiology, 49*, 925–933.

Hoover, R. (2001). Composition, molecular structure, and physicochemical properties of tuber and root starches: A review. *Carbohydrate Polymers, 45*, 253–267.

Huang, J., Shang, Z., Man, J., Liu, Q., Zhu, C., & Wei, C. (2015). Comparison of molecular structures and functional properties of high-amylose starches from rice transgenic line and commercial maize. *Food Hydrocolloids, 46*, 172–179.

Jiranuntakul, W., Puttanlek, C., Rungsardthong, V., Puncha-arnon, S., & Uttapap, D. (2011). Microstructural and physicochemical properties of heat-moisture treated waxy and normal starches. *Journal of Food Engineering, 104*, 246–258.

Larsson, C.-T., Hofvander, P., Khoshnoodi, J., Ek, B., Rask, L., & Larsson, H. (1996). Three isoforms of starch synthase and two isoforms of branching enzyme are present in potato tuber starch. *Plant Science, 117*, 9–16.

Li, H., Dhital, S., Slade, A. J., Yu, W., Gilbert, R. G., & Gidley, M. J. (2019). Altering starch branching enzymes in wheat generates high-amylose starch with novel molecular structure and functional properties. *Food Hydrocolloids, 92*, 51–59.

Lin, L., Zhao, S., Li, E., Guo, D., & Wei, C. (2022). Structural properties of starch from single kernel of high-amylose maize. *Food Hydrocolloids, 124*, Article 107349.

Liu, Q., Donner, E., Tarn, R., Singh, J., & Chung, H.-J. (2009). Chapter 8—Advanced analytical techniques to evaluate the quality of potato and potato starch. In J. Singh, & L. Kaur (Eds.), *Advances in potato chemistry and technology* (pp. 221–248). San Diego: Academic Press.

Lourdin, D., Putaux, J.-L., Potocki-Véronèse, G., Chevigny, C., Rolland-Sabaté, A., & Buléon, A. (2015). Crystalline structure in starch. In Y. Nakamura (Ed.), *Starch: Metabolism and structure* (pp. 61–90). Tokyo: Springer Japan.

Matheson, N. K., & Welsh, L. A. (1988). Estimation and fractionation of the essentially unbranched (amylose) and branched (amylopectin) components of starches with concanavalin a. *Carbohydrate Research, 180*, 301–313.

Nazarian-Firouzabadi, F., & Visser, R. G. F. (2017). Potato starch synthases: Functions and relationships. *Biochemistry and Biophysics Reports, 10*, 7–16.

Nicolia, A., Fält, A.-S., Hofvander, P., & Andersson, M. (2021). Protoplast-based method for genome editing in tetraploid potato. In P. Tripodi (Ed.), *Crop breeding: Genetic improvement methods* (pp. 177–186). New York, NY: Springer US.

Peat, S., Whelan, W., & Thomas, G. J. (1952). Evidence of multiple branching in waxy maize starch. *Journal of The Chemical Society (Resumed)*, 4546–4548. Retrieved from https://www.semanticscholar.org/paper/Evidence-of-multiple-branching-in-waxy-maize-starch-Peat-Whelan/47d3c5d5f521cdcc06a92856fdce6dc1122e59e1.

Pérez, S., Baldwin, P. M., & Gallant, D. J. (2009). Chapter 5—Structural features of starch granules I. In J. BeMiller, & R. Whistler (Eds.), *Starch* (3rd ed., pp. 149–192). San Diego, USA: Academic Press.

Safford, R., Jobling, S. A., Sidebottom, C. M., Westcott, R. J., Cooke, D., Tober, K. J., … Gidley, M. J. (1998). Consequences of antisense RNA inhibition of starch branching enzyme activity on properties of potato starch. *Carbohydrate Polymers, 35*, 155–168.

Seguchi, M., Yasui, T., Hosomi, K., & Imai, T. (2000). Study of internal structure of waxy wheat starch granules by KI/I2 solution. *Cereal Chemistry, 77*, 339–342.

Seung, D. (2020). Amylose in starch: Towards an understanding of biosynthesis, structure and function. *New Phytologist, 228*, 1490–1504.

Seung, D., & Smith, A. M. (2019). Starch granule initiation and morphogenesis—Progress in Arabidopsis and cereals. *Journal of Experimental Botany, 70*, 771–784.

Smith, A. M. (1999). Making starch. *Current Opinion in Plant Biology, 2*, 223–229.

Szydlowski, N., Ragel, P., Raynaud, S., Lucas, M. M., Roldán, I., Montero, M., … Mérida, Á. (2009). Starch granule initiation in Arabidopsis requires the presence of either class IV or class III starch synthases. *The Plant Cell, 21*, 2443–2457.

Tetlow, I. J., & Emes, M. J. (2011). 4.05 - starch biosynthesis in higher plants: The enzymes of starch synthesis. In M. Moo-Young (Ed.), *Comprehensive biotechnology* (2nd ed., pp. 47–65). Burlington: Academic Press.

Tetlow, I. J., & Bertoft, E. (2020). A review of starch biosynthesis in relation to the building block-backbone model. *International Journal of Molecular Sciences, 21*, 7011.

Toinga-Villafuerte, S., Vales, M. I., Awika, J. M., & Rathore, K. S. (2022). CRISPR/Cas9-mediated mutagenesis of the granule-bound starch synthase gene in the potato variety Yukon gold to obtain amylose-free starch in tubers. *International Journal of Molecular Sciences, 23*, 4640.

Tuncel, A., Corbin, K. R., Ahn-Jarvis, J., Harris, S., Hawkins, E., Smedley, M. A., … Smith, A. M. (2019). Cas9-mediated mutagenesis of potato starch-branching enzymes generates a range of tuber starch phenotypes. *Plant Biotechnology Journal, 17*, 2259–2271.

Wang, J., Hu, P., Chen, Z., Liu, Q., & Wei, C. (2017). Progress in high-amylose cereal crops through inactivation of starch branching enzymes. *Frontiers in Plant Science, 8*. Retrieved from https://www.frontiersin.org/articles/10.3389/fpls.2017.00469.

Wang, J., Hu, P., Lin, L., Chen, Z., Liu, Q., & Wei, C. (2018). Gradually decreasing starch branching enzyme expression is responsible for the formation of heterogeneous starch granules. *Plant Physiology, 176*, 582–595.

Wang, S., Li, C., Zhang, X., Copeland, L., & Wang, S. (2016). Retrogradation enthalpy does not always reflect the retrogradation behavior of gelatinized starch. *Scientific Reports, 6*, 20965.

Yamada, T., Komiya, T., Akaki, M., & Taki, M. (1978). A novel type of corn starch from a strain of maize. Part 3. The properties of the starch from Amylo-waxy maize and its hybrids with waxy maize. *Starch - Stärke, 30*, 145–148.

Yun, S.-H., & Matheson, N. K. (1990). Estimation of amylose content of starches after precipitation of maylopectin by Concanavalin-a. *Starch - Stärke, 42*, 302–305.

Zhao, X., Andersson, M., & Andersson, R. (2018). Resistant starch and other dietary fiber components in tubers from a high-amylose potato. *Food Chemistry, 251*, 58–63.

Zhao, X., Andersson, M., & Andersson, R. (2021). A simplified method of determining the internal structure of amylopectin from barley starch without amylopectin isolation. *Carbohydrate Polymers, 255*, Article 117503.

Zhao, X., Hofvander, P., Andersson, M., & Andersson, R. (2023). Internal structure and thermal properties of potato starches varying widely in amylose content. *Food Hydrocolloids, 135*, Article 108148.

Zhao, X., Jayarathna, S., Turesson, H., Fält, A.-S., Nestor, G., González, M. N., … Andersson, M. (2021). Amylose starch with no detectable branching developed through DNA-free CRISPR-Cas9 mediated mutagenesis of two starch branching enzymes in potato. *Scientific Reports, 11*, 4311.

Zhong, Y., Qu, J. Z., Liu, X., Ding, L., Liu, Y., Bertoft, E., … Blennow, A. (2022). Different genetic strategies to generate high amylose starch mutants by engineering the starch biosynthetic pathways. *Carbohydrate Polymers, 287*, Article 119327.

Zhong, Y., Tai, L., Blennow, A., Ding, L., Herburger, K., Qu, J., … Liu, X. (2023). High-amylose starch: Structure, functionality and applications. *Critical Reviews in Food Science and Nutrition, 63*, 8568–8590.